

Photocatalytically active $\text{La}_2\text{Ti}_2\text{O}_7$ nanostructures, synthesis and characterization

Mehdi Rahimi-Nasrabadi^{1,2}  · Saeid Mahdavi² · Kourosh Adib²

Received: 6 March 2017 / Accepted: 4 May 2017 / Published online: 23 May 2017
© Springer Science+Business Media New York 2017

Abstract The major goal of this study was to synthesize $\text{La}_2\text{Ti}_2\text{O}_7$ nanoparticles, using capping agent like cetyltrimethylammonium bromide, sodium dodecyl sulfate, poly vinyl pyrrolidone and glucose. Next the effects of the different agents on the morphology and size of final product particles were evaluated using XRD, SEM, FT-IR, PL and UV-Vis spectroscopy. Further the optimal nano-sized particles were used for the catalysis of light-induced photodegradation of methyl orange under UV irradiation. The results revealed that 95.3% of the pollutant (i.e. methylene blue) was degraded, leading to the decolorization of the samples after 40 min of UV irradiation, in the presence of the particles.

1 Introduction

A prominent modern, and most probably future, challenge is developing clean and efficient energy sources through converting the solar energy to chemical energy. Also energy storage, using devices like supercapacitors, batteries, etc and hence this is a hot area of scientific and R&D activities [1–5]. Controlling environmental pollutants is another a global concern in modern societies [6–8], and in this regard a great deal of attention has been directed to the preparation and evaluation of photocatalysts for use to this end, due to the fact that these compounds are among the

promising technologies aimed at addressing issues of environmental pollutions and clean energy. Photocatalysts can use the solar energy for producing clean energy through the production of hydrogen by degrading pollutants. In this light, various compounds have been prepared and evaluated as photocatalysts [2, 9–12].

Titanium oxide salts of rare earths, generally illustrated as $\text{RE}_2\text{Ti}_2\text{O}_7$ (RE=rare earth) present interesting properties which have changed them to potential candidates for various applications including the area of photocatalysis. These compound have been known to occur in structures [13] based on the size of the cation. For smaller cations like Sm to Lu, the compounds adopt a pyrochlore-like structure with a cubic Fd_3m space group. In the case of the larger cations like La to Nd, however, a non-centrosymmetric monoclinic layered perovskite (LP) structure, P21 space group has been observed [14, 15]. These compounds have been evaluated as photocatalysts [16], dielectric materials [17], components of ferroelectric devices [18], oxygen transport [19] etc. Various lanthanide salts of this family have also proven to have photocatalytic activities in the photo-induced degradation of organic pollutants.

The compounds have been synthesized through different methods like the molten salt [20], sol-gel [21], the polymerized complex [22], auto combustion [23] and pulsed laser deposition [14], stearic acid [24], solid-state reaction [25] methods, many of which suffer problems like the difficulty in controlling the phase of the product, need for large amounts of solvents and high temperatures, and complicated equipment in addition to being time consuming and complicated. Given this, developing facile, rapid and inexpensive procedures for the phase-controlled preparation lanthanide titanates $\text{Ln}_2\text{Ti}_2\text{O}_7$, is a huge challenge. Classically, the sol-gel technique has been found to be advantageous over the solid-state and co-precipitation

✉ Mehdi Rahimi-Nasrabadi
rahiminasrabadi@gmail.com; kpmrahimi@ihu.ac.ir

¹ Faculty of Pharmacy, Baqiyatallah University of Medical Sciences, Tehran, Iran

² Department of Chemistry, Imam Hossein University, Tehran, Iran

approaches, since they enhance the homogeneity of the mixed precursors.

2 Experimental

2.1 Characterization

The X-ray diffraction data were obtained using a Philips-X'PertPro XRD instrument with a Ni-filtered Cu K α radiation. An LEO-1455VP equipped with an energy dispersive X-ray spectroscope was used for obtaining the scanning electron microscopy (SEM) images. An S-10 4100, Scinco UV–Vis scanning spectrometer was used for obtaining the electronic spectra. Energy dispersive spectrometry (EDS) was also conducted using an XL30, Philips microscope. All FT-IR evaluations were conducted on a Bruker Equinox 55 instrument using the KBr pellet method.

2.2 Synthesis of La₂Ti₂O₇ nanoparticles

All chemicals including lanthanum nitrate, ethanol, tetrabutyl titanate (TNBT), cetyltrimethylammonium bromide (CTAB), sodium dodecyl sulfate (SDS), poly vinyl pyrrolidone (PVP) and glucose were obtained from Merck Co. To synthesize the nanoparticles, initially 1 mmol of the surfactant and La(NO₃)₃ was individually dissolved in 5 and 10 mL of distilled water, and then the surfactant solution was added to the cation solution under stirring. Next TNBT was added to this mixture and the stirring was continued until a gel was formed at 110 °C (in the case of ethanol this was observed at 90 °C). This product was next calcinated in a furnace at different temperatures for 3 h in an air atmosphere (Table 1).

2.3 The photocatalytic activity of the nano-particles

The synthesized nanoparticles were assessed as photocatalysts in the photodegradation reaction of methylene blue (MB) in water under UV irradiation. To perform the tests an airlift photoreactor, which was a cylindrical Pyrex double pipe equipped with a high pressure Hg lamp (250 W, λ 280 nm) positioned inside the reactor was used.

A suspension of the photocatalytic nano-particles in the sample solution was prepared by admixing 0.05 g of the particles in 500 mL of 25 mg/L aqueous solutions of MB. Before the onset of the irradiation, the MB concentration as measure through UV–Vis spectrometry and the suspension was mixed in the dark for 20 min. TiO₂ (Degussa P25) was also used as a reference material for comparing the photocatalytic activities of the species. Both the Ln₂Ti₂O₇ and TiO₂ suspensions were subjected to UV light under constant aeration. During the reaction, which was performed under a constant temperature regime at ambient temperature, samples of the solution were taken and their MB concentrations were analyzed at 19 min intervals until 60 min. The measurements of the MB concentrations were performed through UV–Vis spectrometry of the samples at the maximum absorption wavelength of the analytes.

Using the Lambert–Beer law (Eq. 1) [26, 27]:

$$A = \epsilon bC \quad (1)$$

where A, ϵ , b and C illustrate the absorbance of light, the molar absorptivity, the length of path of light through the sample and the concentration of the analyte, the measurements were carried out. Considering A₀ and A_t as the initial absorbance observed for the unreacted sample and the absorbance at time t after the reaction started, and C₀ and C_t as the corresponding concentrations, we have Eq. 2:

$$\text{Degradation efficiency (\%)} = \frac{A_0 - A_t}{A_0} \times 100 \quad (2)$$

Table 1 Preparation conditions for the synthesis of La₂Ti₂O₇ nanoparticles

Sample No.	Solvent	Reaction temperature (°C)	Calcination temperature (°C)	Surfactant	Size of produced La ₂ Ti ₂ O ₇ nanoparticles (nm)
1	Water	110	700	CTAB	90
2	Water	110	700	SDS	135
3	Water	110	700	Glucose	140
4	Ethanol	90	700	CTAB	80
5	Ethanol	90	700	SDS	143
6	Water	110	800	CTAB	126
7	Water	110	900	CTAB	210
8	Ethanol	90	800	CTAB	155
9	Ethanol	90	900	CTAB	200

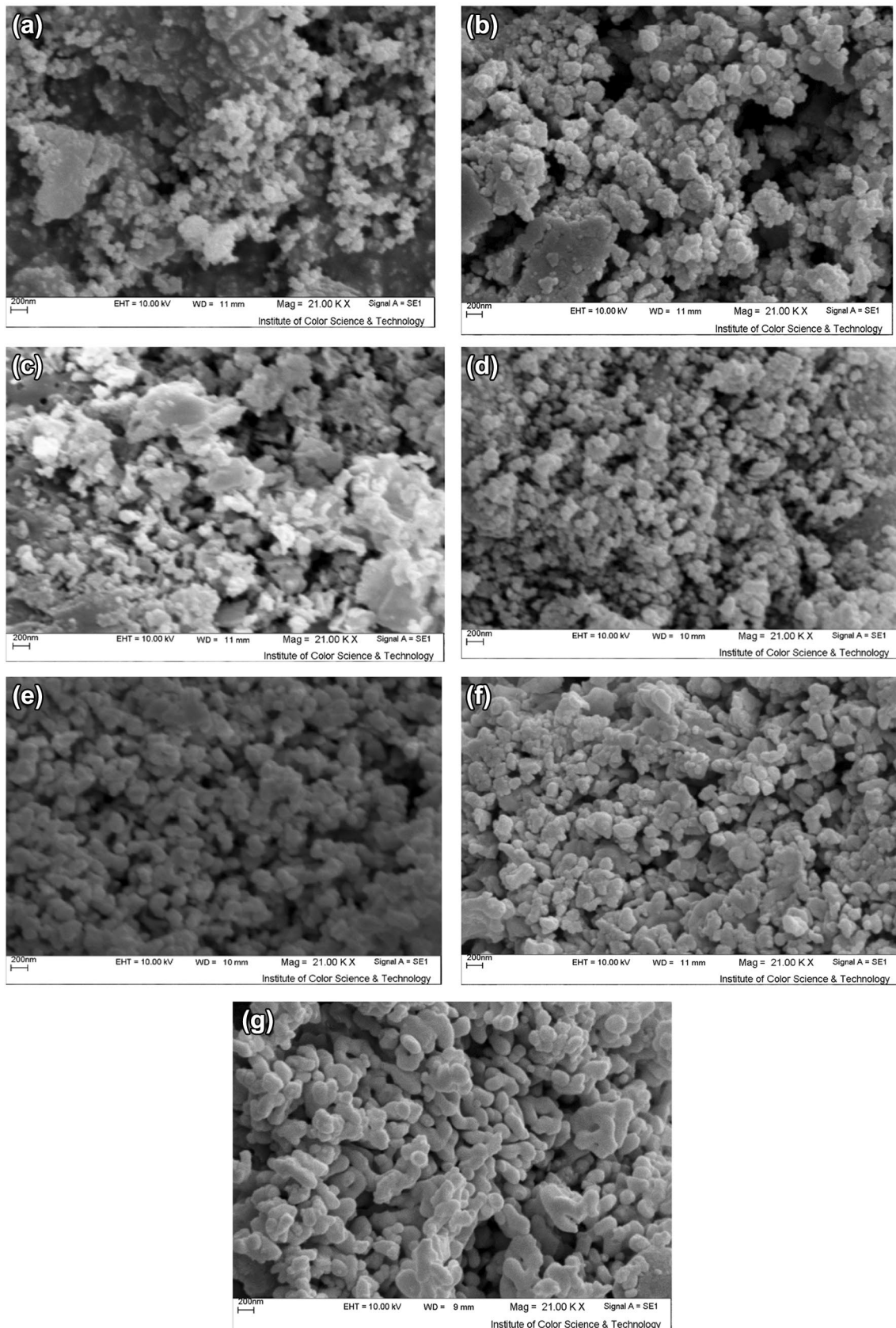


Fig. 1 SEM images of $\text{La}_2\text{Ti}_2\text{O}_7$ nanoparticles prepared under different condition of Table 1; **a** sample 1, **b** sample 2, **c** sample 3, **d** sample 4, **e** sample 5, **f** sample 8, and **g** sample 9

The kinetics of the MB degradation reaction was studied through the Langmuir–Hinshelwood kinetics model. This model is normally used for the photocatalytic degradation of dilute solutions of organic pollutants and is described as the following Equation [31]:

$$-\frac{dC}{dt} = k_{app} C \quad (3)$$

C , k_{app} , t and $-dC/dt$ being the concentration of the pollutant, reaction rate constant, time and reaction rate.

3 Results and discussion

The efforts made in recent years, with the aim of controlling the shape, size and morphology of nanoparticles by manipulating effective reaction parameters, especially given that the properties of nanoparticles greatly depend on their size and shape [29–34]. Accordingly several experiments were performed to study the effects of different parameters. These parameters included the effects of the nature of the surfactants (i.e. CTAB, SDS and glucose) and solvents, as well as the calcination temperature, on the physicochemical properties of $\text{La}_2\text{Ti}_2\text{O}_7$. Figure 1a–c contain the SEM images of the $\text{La}_2\text{Ti}_2\text{O}_7$ samples produced using CTAB, SDS, and glucose in water and calcinated at 700°C , respectively. Figure 1c, shows that using glucose as a surfactant the resulting product mainly consists of agglomerated nanoparticles. The product prepared in the presence of CTAB, on the other hand is smaller in size than that in the presence of SDS (Table 1). These products are nanoparticles with the respective average sizes of around 120 and 135 nm. Since these products have

almost similar properties, both of the surfactants were used while evaluating the solvent.

Next studies were conducted to evaluate the role of the solvent in defining the properties of the product and the results are given in Fig. 1d, e. Based on the results, the $\text{La}_2\text{Ti}_2\text{O}_7$ nanoparticles prepared in ethanol were smaller, as opposed to those prepared in water, in the case of both surfactants. The product in ethanol was less agglomerated as opposed to water, in which due to the fast hydrolysis of the precursor agglomeration is inevitable.

Eventually the product was calcinated at 700 , 800 and 900°C , to determine the optimal calcination temperature and the results are illustrated in Fig. 1f–h. It is evident that particle sizes increased upon increasing the temperature. Yet the sample prepared at 700°C does not possess appropriate crystal properties, and hence 800°C was considered as the optimal calcination temperature.

The crystalline properties of the product samples were studied using XRD. The XRD results obtained for sample 8 is given in Fig. 2. The pattern in this figure was indexed to pure monoclinic $\text{La}_2\text{Ti}_2\text{O}_7$ ($a=13.01 \text{ \AA}$, $b=5.54 \text{ \AA}$, and $c=7.80 \text{ \AA}$) with a P21/m space group according to JCPDS No. 27-1182.

Given that no diffraction peaks corresponding to other species were detected, the samples were considered as being pure. Using the XRD results, the crystallite diameter (D_c) of the optimal nanoparticles (sample 8) was calculated to be 19 nm using the Scherer equation:

$$D_c = K\lambda/\beta \cos \theta$$

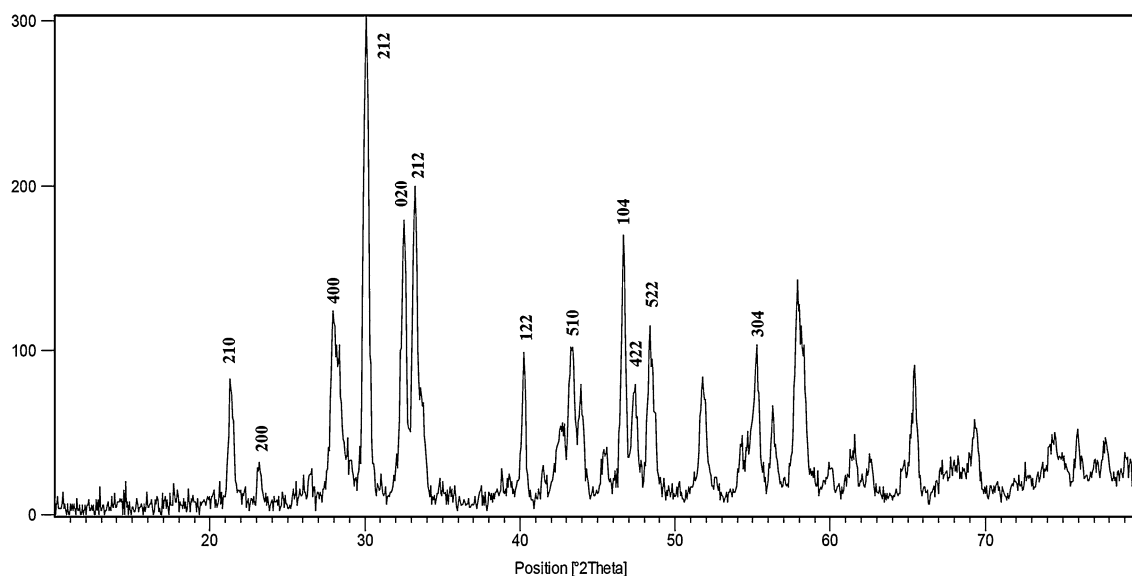


Fig. 2 XRD pattern of $\text{La}_2\text{Ti}_2\text{O}_7$ nanoparticles prepared under optimum condition (sample 8)

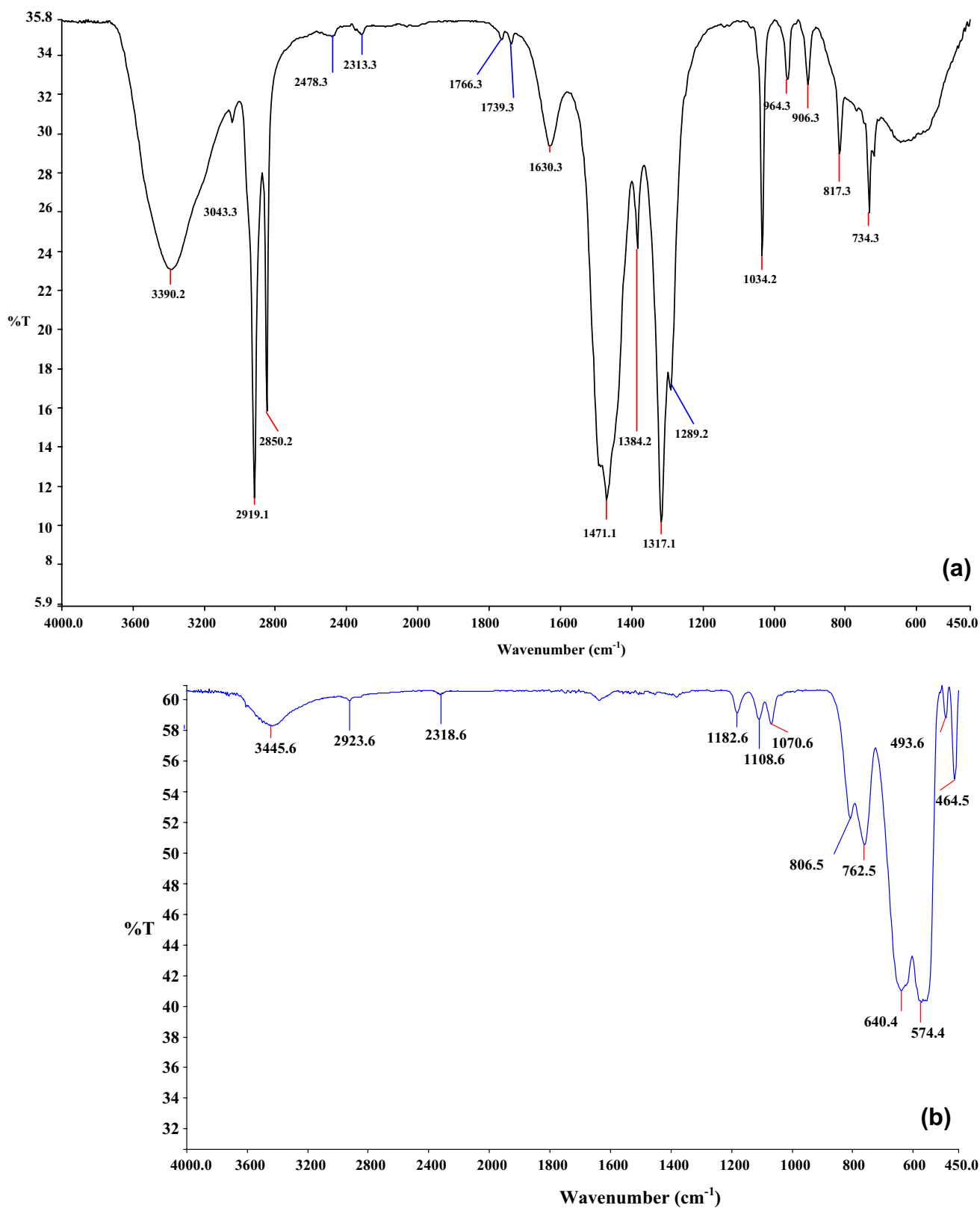


Fig. 3 FT-IR spectra for prepared La₂Ti₂O₇ nanoparticles by sol–gel method at optimum conditions (sample 8) **a** before annealing, and **b** after annealing at 800 °C

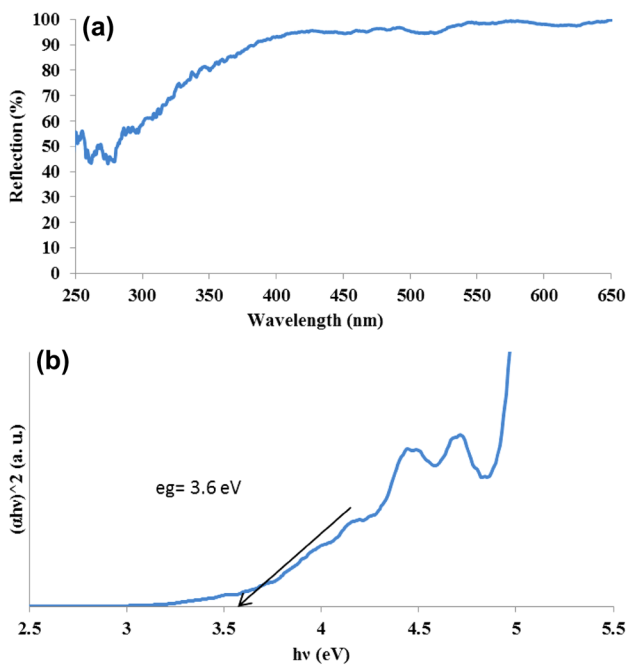


Fig. 4 a Diffuse reflectance UV-Vis spectra of $\text{La}_2\text{Ti}_2\text{O}_7$ nanoparticles. b Tauc's plot for as-prepared $\text{La}_2\text{Ti}_2\text{O}_7$ nanoparticles (sample 8)

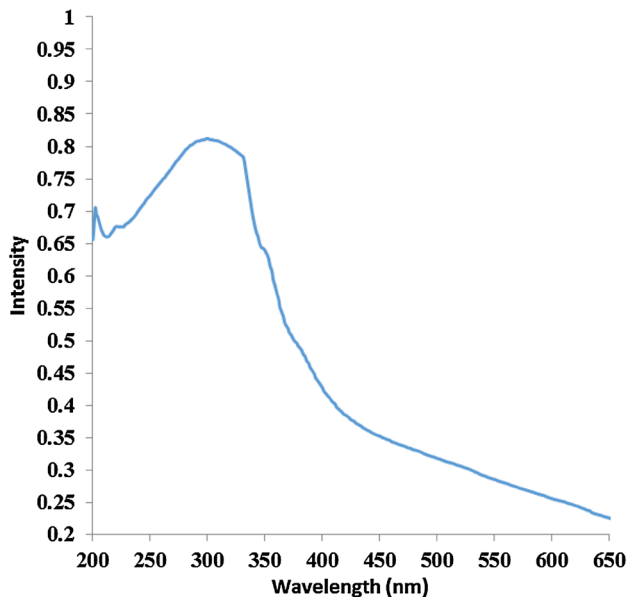


Fig. 5 UV-Vis absorption spectra of the $\text{La}_2\text{Ti}_2\text{O}_7$ nanoparticles prepared via sol-gel method (sample 8)

with β being the breadth of the diffraction line at its half intensity, K being the shape factor (usually around 0.9), and λ being the wavelength of X-ray source [35, 36].

To investigate the presence of functional groups in the structure of the optimal product, the FT-IR spectra of the

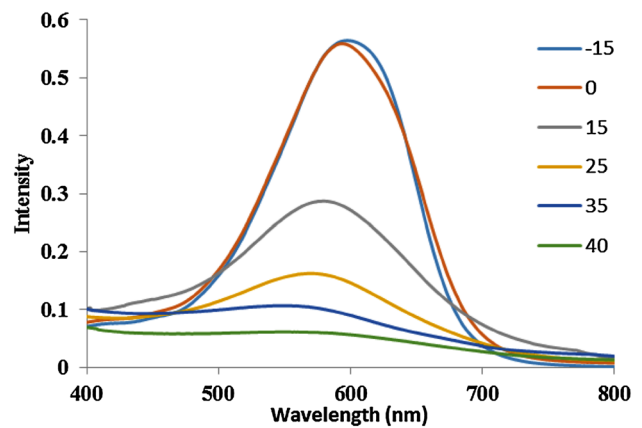


Fig. 6 UV-Vis absorbance spectrum of MB at different time intervals on irradiation using 50 mg $\text{La}_2\text{Ti}_2\text{O}_7$ (sample 8) nanoparticles as photocatalyst

optimal nanoparticles were obtained (Fig. 3). The figure contains the FT-IR spectra of the optimally produced $\text{La}_2\text{Ti}_2\text{O}_7$ nanoparticles both before and after annealing at 800 °C. According to Fig. 3a the absorption peaks at about 734 and 600 cm^{-1} before annealing is related to the stretching vibrations of Ti-O and La-O; respectively. The absorption peak at 3390 and 1470 cm^{-1} in Fig. 5a was attributed to the stretching of the O-H and bending of H-O-H bonds of the water molecules on the external surface of the samples. With calcination of the precipitates at 800 °C, the intensity of this peak was reduced, which supports the idea of the evaporation of adsorbed water (Fig. 3b). Other peaks is related to the presence of surfactant (CTAB) in the sample that the most important of them in the region of 2850 and 2920 cm^{-1} is related to the symmetric and asymmetric stretching vibration of methylene in chain while as can be seen in Fig. 3b after calcination at 800 °C the absorption peaks related to the stretching vibrations of Ti-O and La-O have been splitted and slightly shifted.

The diffused reflectance spectrum of the optimal $\text{La}_2\text{Ti}_2\text{O}_7$ nanoparticles (sample 8) is given in Fig. 4a. In most semiconductors the fundamental absorption edge has an exponential behavior. Based on the absorption data, and using Tauc's equation, the band gap was determined:

$$(\alpha h\nu)^{1/n} = A(h - E_g)$$

h , ν , α , E_g , and A being Planck's constant, frequency of light, absorption coefficient, band gap energy and a constant value, respectively. n , can be 0.5 and 2 depending on the transition mechanism and was considered 0.5, here. The band gap energy for the optimal $\text{La}_2\text{Ti}_2\text{O}_7$ nanoparticles was determined through extrapolating the linear sections of a plot of $(\alpha h\nu)^2$ against $h\nu$ (Fig. 4b), and was found to be 3.6 eV [11].

To evaluate the absorption profile of the optimal product UV–Vis spectroscopy was used to study the behavior of a dispersion of the $\text{La}_2\text{Ti}_2\text{O}_7$ nanoparticles in distilled water and the results (Fig. 5) shows the main absorption in the region of 200–350 nm. This can be held as proof of the small size of the particles, due to the strong quantum confinement of the excitonic transition for nano-structures [37–39].

3.1 Photocatalytic activity

The results of tests on the photodegradation of aqueous methylene blue (MB) solutions under UV light and in the presence of the synthesized $\text{La}_2\text{Ti}_2\text{O}_7$ (Fig. 6) were found to be very promising. Figure 7a is a plot of MB concentration in the aqueous solution in the presence of $\text{La}_2\text{Ti}_2\text{O}_7$ and TiO_2 nanoparticles (C/C_0 versus illumination time). $\text{La}_2\text{Ti}_2\text{O}_7$ nanoparticles were found to

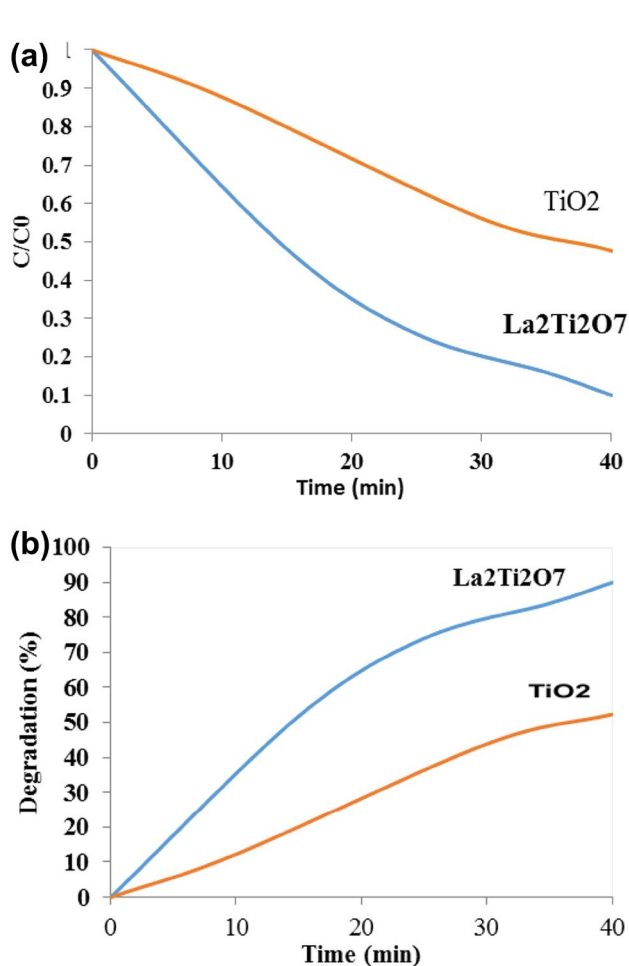


Fig. 7 **a** Comparison of photocatalytic behavior, and **b** photocatalytic degradation of methylene blue solution under UV irradiation using $\text{La}_2\text{Ti}_2\text{O}_7$ (sample 8) and TiO_2

effectively degrade MB. Based on Fig. 7b, which is a plot of the degradation percentage over time, after 40 min the maximum conversion is reached. The maximum conversion was calculated to be about 95.3 in the presence of the $\text{La}_2\text{Ti}_2\text{O}_7$ nanoparticle while it was 50% for and TiO_2 nanoparticles.

Figure 8 further illustrates the pseudo 1st order kinetics of the photodegradation reaction in the presence of the $\text{La}_2\text{Ti}_2\text{O}_7$ nanoparticles, and the slope of the linear regression can yield the first-order reaction rate constant. Overall, the observations proved that $\text{La}_2\text{Ti}_2\text{O}_7$ can effectively degrade MB, at higher speeds as compared to TiO_2 . This shows that the $\text{La}_2\text{Ti}_2\text{O}_7$ nanoparticles can act as superior photocatalysts with promising qualities to be used in the photocatalytic removal of organic pollutions from water samples.

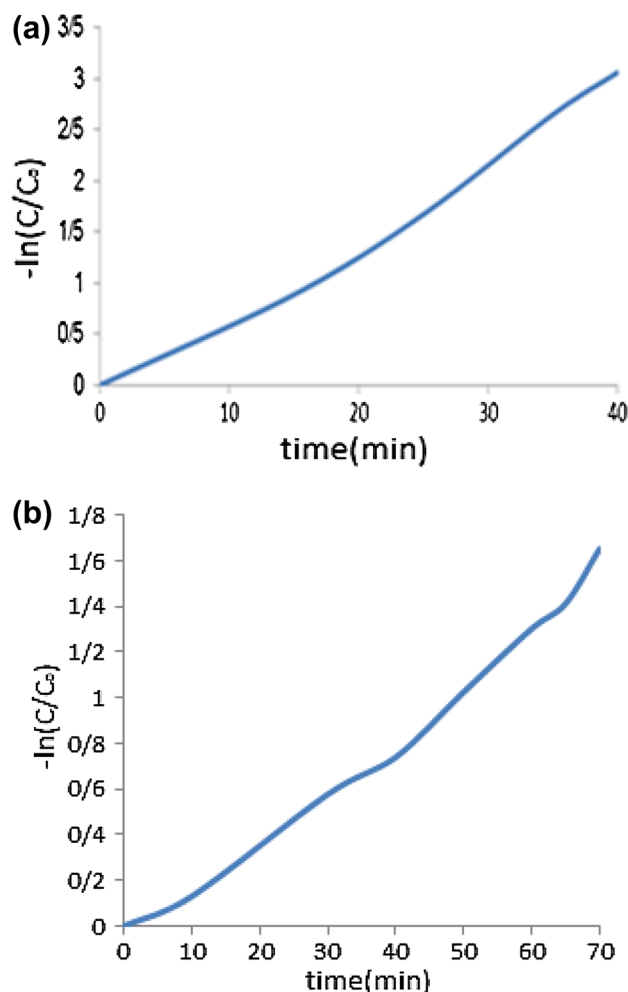


Fig. 8 Pseudo first order kinetics of MB degradation for: **a** $\text{La}_2\text{Ti}_2\text{O}_7$ and **b** TiO_2

4 Conclusion

After the successful synthesis of $\text{La}_2\text{Ti}_2\text{O}_7$ nanoparticles through a facile procedure, and evaluating the effects of capping agents, solvent and calcinations temperature on the physic chemical properties of the products, various tests were performed using CTAB, SDS, PVP and glucose. The different $\text{La}_2\text{Ti}_2\text{O}_7$ nanoparticles were analyzed through XRD, UV–Vis, FT-IR and SEM, and also evaluated as photocatalysts with a maximal methylene blue degradation yield of about 95.3% after 40 min under UV light.

Funding The authors are gratefully acknowledged the financial support provided by Iran National Science Foundation (Project 94019559).

References

- M. Rahimi-Nasrabadi, H.R. Naderi, M. Sadeghpour Karimi, F. Ahmadi, S. M. Pourmortazavi, J. Mater. Sci. Mater. Electron. **28**, 1877 (2017)
- M. Rahimi-Nasrabadi, J. Mater. Sci. Mater. Electron. **28**, 2200 (2017)
- M. Shamsipur, S. M. Pourmortazavi, M. Roushani, I. Kohsari, S.S. Hajimirsadeghi, Microchim. Acta. **173**, 445 (2001)
- M. Pirhashemi, A. Habibi-Yangjeh, J. Mater. Sci. Mater. Electron. **27**, 4098 (2016)
- M. Pirhashemi, A. Habibi-Yangjeh, J. Colloid Interface Sci. **474**, 103 (2016)
- M. Rahimi-Nasrabadi, M.M. Zahedi, S.M. Purmortazavi, J. Jazayeri, Microchim. Acta **177**, 145 (2012)
- M.M. Zahedi, M. Rahimi-Nasrabadi, S.M. Pourmortazavi, G.R. Fallah Koohbijari, J. Shamsi, M. Payravi, Microchim. Acta **179**, 57 (2012)
- M. Rahimi-Nasrabadi, F. Ahmadi, M. Eghbali-Arani, J. Mater. Sci. Mater. Electron. **28**, 2415 (2017).
- B. Golzad-Nonakaran, A. Habibi-Yangjeh, Adv. Powder Technol. **27**, 1427 (2016)
- S. Vadivel, D. Maruthamani, B. Paul, S.S. Dhar, A. Habibi-Yangjeh, S. Balachandran, B. Saravanakumar, A. Selvakumar, K. Selvam, RSC Adv. **6**, 74177 (2016)
- F. Ahmadi, M. Rahimi-Nasrabadi, M. Behpour, J. Mater. Sci. Mater. Electron. **28**, 1531 (2017)
- M. Rahimi-Nasrabadi, F. Ahmadi, A. Fosooni, J. Mater. Sci. Mater. Electron. **28**, 537 (2017)
- A.V. Prasadarao, U. Selvaraj, S. Komarneni, A.S. Bhalla, Mater. Lett. **12**, 306 (1991)
- A. Bayart, S. Saitzek, A. Ferri, R. Pouhet, M. Chambrier, P. Roussel, R. Desfeux, Thin Solid Films **553**, 71 (2014)
- A.V. Shlyakhtina, A.V. Knotko, M.V. Boguslavskii, S.Y. Stefanovich, D.V. Peryshkov, I.V. Kolbanev, L.G. Shcherbakova, Solid State Ionics **176**, 2297 (2005)
- W. Zhang, Z. Ma, L. Du, L. Yang, H. He, J. Alloys Compd. **695**, 3541 (2017)
- V.V. Nemoshkalenko, V.N. Uvarov, S.V. Borisenko, A.I. Senkevich, T.N. Bondarenko, J. Electron Spectrosc. Relat. Phenom. **385**, 88 (1998)
- V.V. Atuchin, T.A. Gavrilova, J.C. Grivel, V.G. Kesler, Surf. Sci. **602**, 3095 (2008)
- A.V. Shlyakhtina, A.V. Knotko, M.V. Boguslavskii, S.Yu. Stefanovich, D.V. Peryshkov, I.V. Kolbanev, L.G. Shcherbakov, Solid State Ionics **176**, 2297 (2005)
- D. Arney, B. Porter, B. Greve, P.A. Maggard, J. Photochem. Photobiol. A **199**, 230 (2008)
- Z.M. Shao, S. Saitzek, P. Roussel, O. Mentre', F.P. Gheorghiu, L. Mitoseriu, R. Desfeux, J. Solid State Chem. **183**, 1652 (2010)
- W. Hou, Y. Ku, J. Alloys Compd. **509**, 5913 (2011)
- H. Xue, Y. Zhang, J. Xu, X. Liu, Q. Qian, L. Xiao, Q. Chen, Catal. Commun. **51**, 72 (2014)
- W. Zhang, L. Zhang, H. Zhong, L. Lu, X. Yang, X. Wang, Mater. Charact. **61**, 154 (2010).
- M. Uno, A. Kosuga, M. Okui, K. Horisaka, S. Yamanaka, J. Alloys Compd. **400**, 270 (2005)
- M. Rahimi-Nasrabadi, S.M. Pourmortazavi, M.R. Ganjali, P. Novrouzi, F. Faridbod, M. Sadeghpour Karimi, J. Mater. Sci. Mater. Electron. **28**, 3325 (2017)
- M. Rahimi-Nasrabadi, J. Mater. Sci. Mater. Electron. (2016). Doi:[10.1007/s10854-016-6321-4](https://doi.org/10.1007/s10854-016-6321-4)
- M. Rahimi-Nasrabadi, S.M. Pourmortazavi, M.R. Ganjali, P. Norouzi, F. Faridbod, M. Sadeghpour Karimi, J. Mater. Sci. Mater. Electron. **27**, 12860 (2016)
- M. Rahimi-Nasrabadi, F. Ahmadi, S. Hamdi, N. Eslami, K. Didehban, M.R. Ganjali, J. Mol. Liq. **216**, 814 (2016)
- M. Rahimi-Nasrabadi, S.M. Pourmortazavi, M. Khalilian-Shalamzari, J. Mol. Struct. **1083**, 229 (2015)
- M. Rahimi-Nasrabadi, M. Behpour, A. Sobhani-Nasab, S.M. Hosseinpour-Mashkani, J. Mater. Sci. Mater. Electron. **26**, 9776 (2015)
- S.M. Pourmortazavi, S.S. Hajimirsadeghi, M. Rahimi-Nasrabadi, Mater. Sci. Semicond. Process. **16**, 131 (2013)
- S.M. Pourmortazavi, S.S. Hajimirsadeghi, M. Rahimi-Nasrabadi, I. Kohsari, Synth. React. Inorg. Met.-Org. Chem. **42**, 746 (2012)
- Iraj Kohsari, Zahra Shariatinia, SeiedMahdi Pourmortazavi, Carbohydr. Polym. **140**, 287 (2016)
- M. Rahimi-Nasrabadi, M. Rostami, F. Ahmadi, A. Fallah Shojajaie, M. Delavar Rafiee, J. Mater. Sci. Mater. Electron. **27**, 11940 (2016)
- M. Rahimi-Nasrabadi, F. Ahmadi, M. Eghbali-Arani, J Mater Sci. **27**, 13294 (2016)
- M. Rahimi-Nasrabadi, S.M. Pourmortazavi, M.R. Ganjali, S.S. Hajimirsadeghi, M.M. Zahedi, J. Mol. Struct **1047**, 31 (2013)
- M. Rahimi-Nasrabadi, S.M. Pourmortazavi, S.A.S. Shandiz, F. Ahmadi, H. Batooli, Nat. Prod. Res **28**, 1964 (2014)
- S.M. Pourmortazavi, M. Rahimi-Nasrabadi, Y. Fazli, M. Mohammad-Zadeh, Int. J. Refract. Met. Hard Mater. **51**, 29 (2015)